CHMP2A regulates broad immune cell-mediated antitumor activity in an immunocompetent in vivo head and neck squamous cell carcinoma model

Jiyoung Yun [1,2,3] Robert Saddawi-Konefka [1,4] Benjamin Goldenson,[1,2,3] Riyam Al-Msari,[1] Davide Bernareggi,[2] Jaya L Thangaraj,[2,3] Shiqi Tang,[1] Sonam H Patel,[1] Sarah M Luna,[1] J Silvio Gutkind,[1,5] Dan Kaufman [1,2,3]

[1]Moores Cancer Center, University of California-San Diego, La Jolla, California, USA
[2]Dept. of Medicine, University of California-San Diego, La Jolla, California, USA
[3]Sanford Stem Cell Institute, University of California-San Diego, La Jolla, California, USA
[4]Dept. of Otolaryngology-Head and Neck Surgery, University of California-San Diego, La Jolla, California, USA
[5]Dept. of Pharmacology, University of California School of Medicine, La Jolla, California, USA

Correspondence to
Dr Dan Kaufman;
dskaufman@ucsd.edu

ABSTRACT

Background Natural killer (NK) cells are key effector cells of antitumor immunity. However, tumors can acquire resistance programs to escape NK cell-mediated immunosurveillance. Identifying mechanisms that mediate this resistance enables us to define approaches to improve immune-mediate antitumor activity. In previous studies from our group, a genome-wide CRISPR-Cas9 screen identified Charged Multivesicular Body Protein 2A (*CHMP2A*) as a novel mechanism that mediates tumor intrinsic resistance to NK cell activity.

Methods Here, we use an immunocompetent mouse model to demonstrate that CHMP2A serves as a targetable regulator of not only NK cell-mediated immunity but also other immune cell populations. Using the recently characterized murine 4MOSC model system, a syngeneic, tobacco-signature murine head and neck squamous cell carcinoma model, we deleted mCHMP2A using CRISPR/Cas9-mediated knock-out (KO), following orthotopic transplantation into immunocompetent hosts.

Results We found that mCHMP2A KO in 4MOSC1 cells leads to more potent NK-mediated tumor cell killing in vitro in these tumor cells. Moreover, following orthotopic transplantation, KO of mCHMP2A in 4MOSC1 cells, but not the more immune-resistant 4MOSC2 cells enables both T cells and NK cells to better mediate antitumor activity compared with wild type (WT) tumors. However, there was no difference in tumor development between WT and mCHMP2A KO 4MOSC1 or 4MOSC2 tumors when implanted in immunodeficient mice. Mechanistically, we find that mCHMP2A KO 4MOSC1 tumors transplanted into the immunocompetent mice had significantly increased CD4+T cells, CD8+T cells. NK cell, as well as fewer myeloid-derived suppressor cells (MDSC).

Conclusions Together, these studies demonstrate that CHMP2A is a targetable inhibitor of cellular antitumor immunity.

INTRODUCTION

Natural killer (NK) cells are a key part of the innate immune system and possess intrinsic killing activity against tumors without prior antigen priming.[1][2] NK cells comprise 5%–15% of peripheral blood lymphocytes

WHAT IS ALREADY KNOWN ON THIS TOPIC

⇒ A previous natural killer (NK) cell-based two cell type screen identified CHMP2A as a key inhibitor of NK cell-mediated antitumor activity.

WHAT THIS STUDY ADDS

⇒ These current studies now deleted CHMP2A in murine head and neck squamous cancer cell tumor cell lines that were tested in syngeneic immunocompetent mice. This approach enables us to better characterize more diverse immune cells that are affected by CHMP2A-mediated immune suppression.

HOW THIS STUDY MIGHT AFFECT RESEARCH, PRACTICE OR POLICY

⇒ Targeting CHMP2A and/or other members of the ESCRTIII complex provides a novel approach for specific new therapies that can block this immune-inhibitory mechanism and improve immune cell-mediated therapies.

and are characterized as CD3⁻CD56+ lymphocytes in humans and CD3⁻ NK1.1+NKp46+ in mice.[3][4] While T cells recognize antigen peptides presented on the surface of the major histocompatibility complexes (MHC) through their T cell receptors (TCRs),[5–8] NK cells do not rely on a TCR for their activation.[9][10] Instead, NK cell responses are controlled by multiple signals from diverse inhibitory and activating receptors.[9][11] NK cells sense HLA class I molecules via inhibitory killer cell immunoglobulin-like receptors (KIRs) and the inhibitory signaling from KIRs blocks NK cell-mediated killing.[6][12] Tumor cells that downregulate MHC I to avoid T cell-mediated immune surveillance are recognized by NK cells, which, in turn, selectively target those tumor cells with absent MHC I molecules due to recognition of these 'missing self' targets.[9][13–15] Despite the variety of receptors NK cells possess to detect tumors, tumor

cells become resistant to and escape NK cell-mediated immune surveillance by various mechanisms.[16 17]

A previous study from our group conducted CRISPR/Cas9-mediated two-cell type screen to identify CHMP2A as novel a gene that mediates tumor cell resistance to NK cell-mediated cytotoxicity.[18] CHMP2A is a member of the ESCRTIII complex and regulates the secretion of tumor-derived chemokines and extracellular vehicles (EVs).[19–21] Specifically, CHMP2A mediates secretion of EVs expressing NK cell activating ligands such as MHC class I chain-related proteins A and B (MICA/B), which act as a decoy to inhibit NK cells killing of tumor cells.[18 19 22 23] Tumor cells modify the tumor microenvironment (TME) to become immunosuppressive by secreting EVs expressing MHC Class I, MICA/B, and ligands for NK cell activating receptor NK group2 member D (NKG2D).[24–26] Expression of MICA/B on the surface of EVs inhibits NK cell-mediated antitumor activity.[27 28] In addition, these EVs also express tumor necrosis factor-related apoptosis-inducing ligand (TRAIL) or Fas ligand (FasL) which induce apoptosis in NK cells.[18] These studies demonstrated that deletion of CHMP2A in both glioblastoma and head and neck squamous cancer cell (HNSCC) tumors increases allogeneic NK cell-mediated killing both in vitro and in vivo using a xenograft mouse model.[18] Other recent studies demonstrate the ESCRT complex can repair T cell-mediated perforin holes in tumor cells to delay or prevent T cell-induced killing.[29] Therefore, CHMP2A and the ESCRT complex enable a broader mechanism of resistance to immune cell-mediated antitumor activity.

HNSCC is one of the most aggressive solid tumors leading to its high mortality, morbidity, and risk for recurrence.[30 31] Furthermore, HNSCC is among the most highly immune-infiltrated cancer types, yet response rates to T cell checkpoint inhibitor immunotherapies are typically low.[30–33] Studies of NK cell-mediated antitumor activity against HNSCC demonstrate that a higher infiltration of NK cells into these tumors correlates significantly with the patient's prognosis and survival.[34 35]

While our previous studies identified the ability of CHMP2A to inhibit NK cell-mediated antitumor activity in an NSG xenograft model,[18] we now used a murine syngeneic model to analyze the broader role of mCHMP2A on HNSCC antitumor activity in vivo using immune competent mice.[36–38] 4MOSC1 and 4MOSC2 cells were derived by exposure to 4-nitroquinoline-1 oxide, a tobacco-associated carcinogen, on the tongue of C57Bl/6 mice.[36 38] Previously, we demonstrated that the 4MOSC1 tumors respond to anti-CTLA-4 treatment while the more immune-resistant 4MOSC2 tumors failed to respond to anti-CTLA-4 treatment.[36] Here, we deleted the *mCHMP2A* gene in the 4MOSC1 and 4MOSC2 HNSCC lines and then implanted wild type (WT) or 4MOSC1 and 4MOSC2 mCHMP2A knock-out (KO) cells orthotopically into the tongues of immunocompetent C57BL/6 mice. Mice injected with 4MOSC1 mCHMP2A-KO cells (though not 4MOSC2 mCHMP2A-KO cells) showed a significant decrease in tumor volume and increased immune cell infiltration when compared with mice injected with 4MOSC1-WT cells. However, when injected into immunodeficient NSG mice, there was no difference in tumor growth of the mCHMP2A-KO compared with WT cells for either the 4MOSC1 or 4MOSC2 tumors. Together, these studies demonstrate that mCHMP2A plays an important role in immune cell-mediated antitumor activity of immune-sensitive tumors in vivo.

MATERIALS AND METHODS
Cell culture
4MOSC1 WT and 4MOSC2 WT cell lines were derived as previously described[36] and were cultured in Defined Keratinocyte SFM (ThermoFisher #10744019) supplemented with 5 ng/mL EGF Recombinant Mouse Protein (Thermofisher # PMG8041), 0.0001 nM/mL Cholera Toxin (Sigma-Aldrich, #C8052), and 1% penicillin/streptomycin (Sigma-Aldrich #A5955).

CRISPR-Cas9 gene editing
mCHMP2A-KO was performed on 4MOSC1 and 4MOSC2 cells using the RNP complex protocol provided by Integrated DNA Technologies (IDT; Coralville, Iowa, USA). (Alt-R CRISPR-Cas9 system, IDT). Three CRISPR RNAs (crRNAs) targeting exon 1 of the mCHMP2A gene: crRNA#1, CCAACGACAACCCCTCGGTT; crRNA#2, GTACGCTTGAGTAGTCAAAA; crRNA #3: GTTGTGAGGCCCCTCGACAA were used. RNA oligos are purchased from IDT and resuspended in 1×Tris EDTA (TE), PH 8, solution (IDT, Coralville) to the desired concentration of 200 µM. Designed crRNAs were synthesized with nonspecific Alt-R CRISPR-Cas9 tracrRNA ATTO 550 (IDT #1075927) into gRNAs. 8×10⁵ 4MOSC1 and 4MOSC2 cells were each nucleofected using the Amaxa 2D nucleofector (Lonza) and Mouse Neural Stem Cell Nucleofector Kit (Lonza #VAPG-1004) following the manufacturer's protocol. After nucleofection, cells were seeded in Matrigel coated plates. 48 hours after nucleofection, cells were plated into Matrigel coated 96 well plates using the limiting dilution method (Corning, Massachusetts, USA). Single clones were collected and deletion of mCHMP2A was assessed by PCR and immunoblotting.

PCR gel electrophoresis
DNA from 4MOSC1 and 4MOSC2 cells was extracted and purified using the QIAamp DNA Blood Mini (Qiagen #51104). For PCR amplification, primers spanning the Cas9-single-guide RNA cleavage site of exon 1 of the mCHMP2A gene were used: exon 1 forward primer, TAGCACTTCCCAGCATTCCCGGA; exon 1 reverse primer, TGCTGGTGGAGTCTTACCACCATGG and GoTaq green Master Mix (Promega #M7122) were used.

Immunoblotting
Immunoblotting was performed according to Invitrogen protocols for Mini Gel Tank and iBlot 2 dry system (Thermo

Fisher Scientific #IB21001). Briefly, cell lysates were prepared by incubating cells with RIPA buffer (Thermo Fisher Scientific #89900) containing Halt Protease Inhibitor Cocktail (Thermo Fisher Scientific #87786) and quantified using Pierce BCA assay (Thermo Fisher Scientific #23227). 20 µg of protein lysate was loaded on each gel well. Proteins were separated using NuPAGE Bis-Tris 4%–12% gels (Thermo Fisher Scientific # NP0321BOX) and transferred to nitrocellulose membranes using the iBlot2 dry method. Membranes were blocked for 40 min in 4% milk and incubated with the primary CHMP2A Antibody (1:600) (Proteintech #10477-1-AP) in 4% milk overnight at 4°C. After incubating the membrane with the appropriate secondary antibody conjugated to horse-radish peroxidase (1:10,000) (Goat anti-Rabbit IgG, ThermoFisher #31460), protein levels were detected using Immobilon Western Chemiluminescent HRP Substrate (EMD Millipore # WBKLS0500). CHMP2A overexpression 7 lysate (OL) control used in Supplemental figure 1C was purchased from Origene # LC404873.

Mouse NK cell isolation

Five C57Bl/6 mice were injected with 200 µg of poly I:C per injection and resuspended in sterile water (Invivogen #tlrl-picw) 1 day before isolating NK cells. Spleens from C57Bl/6 mice were collected and minced into fibrous tissue using a plunger. Splenocytes were collected with 5 mL of DMEM and passed through into a 100 µm cell strainer. 5 mL of ACK lysing buffer (Gibco #A1049201) was added and mixed for 5 min to lyse red blood cells. Then, mouse NK cells were isolated using EasySep Mouse NK cell isolation kit (Stemcell Technologies #19855), and flow cytometric analyses were performed to determine the percentage of NK1.1 positive NK cells.

Mouse NK cell cytotoxicity assay

Target cells were prestained with CellTrace Violet (Thermo Fisher Scientific #C34557) at a concentration of 5 mM in PBS for 15 min at 37°C. Target cells were incubated in a complete culture medium containing Fetal Bovine Serum (FBS) for 5 min and harvested by centrifugation. Target cells were resuspended in culture media before being mixed with mouse NK cell cultures at the indicated effector to target ratios. Co-cultures were incubated at 37°C and after 3.5 hours CellEvent Caspase-3/7 Green Detection Reagent (Thermo Fisher Scientific #C10423) and SYTOX AADvanced dead cell stain solution (Thermo Fisher Scientific #S10349) were added for an additional 30 min of culture for a total incubation time of 4 hours. Cells were then analyzed by flow cytometry. Mouse NK cell killing was calculated by subtracting the background of untreated target cells from all the other samples of the same experimental group.

In vivo mouse experiments and analysis

All mice were housed, treated, and handled in accordance with the guidelines set forth by the University of California, San Diego Institutional Animal Care and Use Committee (IACUC, Ref# S16082) and the National Institutes of Health's Guide for the Care and Use of Laboratory Animals. 4MOSC1 and 4MOSC2 cells were transplanted (1×10^6 cells per mouse) into the tongue of 4–6 weeks old female C57Bl/6 mice and NOD.Cg-Prkdc^{scid}IL2rg^{tm1Wjl}/Sz (NSG) mice (Jackson Laboratories), as previously described[36 37]. Tumor volume was monitored using calipers every 2–3 days. Mice were euthanized when necrosis of tongue tumor tissue was observed or at the experiment endpoint. For drug treatment, the mice were treated by intraperitoneal injection with anti-CD4 (Clone GK1.5), anti-NK1.1,(Clone PK136) or anti-CD8 antibody (Clone YTS 169.4, Bio X Cell) (10 mg/kg) on the day of tumor implantation (day 0), 2 days after implantation (day 2), 4 days after implantation (day 4) and then every 4 days thereafter. The mice were then euthanized after the completion of the treatment (or when control-treated mice showed tumor necrosis)

Tissue isolation and flow cytometry

Tumors and other tissues were isolated and stained following the previously established protocols[36–38] on day 10 of injection. Briefly, tumors, spleen, and lymph nodes were dissected, minced, and mechanically digested in Tumor Dissociation Kit, mouse (Miltenyi Biotec #130-096-730) in combination with the gentleMACS dissociator (Milteny Biotec #130-093-235). In case of tumors, tongue tissue was first dissected. Then, the parts of tongue containing tumor were further dissected for indicated procedures. Tumor and tissue suspensions were washed with media and passed through a 100 µm cell strainer. Cells were washed with PBS and immediately processed for live/dead cell staining and cell surface staining. Staining was done for 30 min at 4°C with the following antibodies (Biolegend, used at 1:100 unless specified): CD45 BUV496 (748371, clone 30-F11), Slamf6-Pacific Blue (134608, clone 330-AJ), PD-1 BV510 (135241, clone 29F.1A12), CD8 BV711 (100747, clone53-6.7), CD44 BV785 (100747, clone IM7), CD3 FITC (100204, clone 17A2), CD4 BB700 (745922, clone GK1.5), CD19 PE (553786, clone 1D3), CXCR3 PE Dazz (745922, clone S18001A), Tim3 PECy7 (119716, clone RMT3-23), NK1.1 APC (108710, clone PK136), CD62L APC Cy7 (104428, clone MEL-14), XCR1- BV421 (148216, clone ZET), CD11b BV711 (101242, clone N418), MHCII PECy5 (107626, clone M5/114.15.2, 1:200), Ly6C PE (128008, clone HK1.4), CD64 PE Dazz (139320, clone X54-5/7.1), Ly6G PECy7 (127618, clone 1A8), PD-L1 APC (124312, clone 10F.9G2), CD103 APC Cy7 (121432, clone 2E7). Flow cytometry data acquisition was done using BD LSRFortessa and analyzed using FlowJo. Immune cells were identified by the following markers: cytotoxic T cells (CD45$^+$CD3$^+$CD8$^+$), helper T cells (CD45$^+$CD3$^+$CD4$^+$), NK cells (CD45$^+$NK1.1$^+$CD3$^-$), and PMN-myeloid-derived suppressor cell (MDSCs) (CD45$^+$NK1.1$^-$CD11b$^+$CD11c$^-$Ly-6C^{low}Ly6G$^+$). Gating strategy for flow cytometry is shown in online supplemental figure 6.

IMMUNOFLUORESCENCE ANALYSIS

4MOSC1 and 4MOSC2 cells were transplanted (1×10^6 cells per mouse) into the tongue of 4–6 weeks old female C57Bl/6 mice. On day 10, tongue tissue with area of tumor injection was harvested, fixed, and embedded in paraffin. Staining was performed on intellipath automated IHC stainer (Biocare). Slides were stained for anti-CD3 (Rabbit, Abcam, ab16669, 1:500), anti-NK 1.1 (Mouse, Thermofisher, MA1-70100, 1:100), and anti-CD11b (Rat, Invitrogen 14-0112-82, 1:500) for 1 hour. Stained slides were scanned with Fluorescent PhenoImager (Akoya Biosciences) and Phenochart (Akoya Biosciences) software was used for image analysis.

Chemokine expression profile

Tongue tumors were dissected and lysed in RIPA lysis buffer supplemented with protease and phosphatase inhibitors.[36] Samples were analyzed on the Mouse Chemokine Array (EveTechnologies, Canada).

EVs harvesting and analysis

On day 1, WT or mCHMP2A KO cells were resuspended in Defined Keratinocyte SFM and 0.5×10^6 cells were plated on 100 mm cell culture dishes and cultured at 37°C for 3 days. On day 3, conditioned media were collected and centrifuged at 3000×g for 15 min to remove cell debris. 1:5 ExoQuick ULTRA EVs Isolation Kit for Tissue Culture Media (SBI System Biosciences) was added to the collected media and incubated overnight at 4°C. On day 4, the media was centrifuged at 3000×g for 10 min, supernatant was removed and the pellet was resuspend in 1 mL of 0.22 µm filtered PBS. Isolated EVs were incubated with primary staining with mRae (AF1136-SP, R&D Systems) mULBP (MAB2588-SP, R&D Systems), and mH60 (MAB1155-SP, R&D Systems) for 30 min on ice and washed with flow buffer. Samples were then stained with anti-Rat IgG PE-conjugated secondary antibody for 30 min on ice and were resuspended in 200 µL flow buffer for flow cytometric analysis. The size and number of collected EVs were analyzed by ViewSizer 3000 (HORIBA scientific).

STATISTICAL ANALYSIS

For in vitro assays, experimental conditions were run as biological triplicates and experimental duplicates. All experiments were combined for statistical analysis. For in vivo experiments, each independent experiment included five mice per group. All data are represented as means and error bars as SD. For correlation analysis, the immune infiltration rate was plotted against tumor volume and the best-fit line and correlation coefficient value (R^2) was calculated through GraphPad Prism. All statistical analysis was analyzed through GraphPad Prism software.

RESULTS
Deletion of mCHMP2A in the 4MOSC1 and 4MOSC2 HNSCC lines

Previous studies from our group identified human CHMP2A as a novel regulator of NK cell-mediated antitumor activity in diverse solid tumors.[18] Here, we aimed to test the role of mCHMP2A in an immunocompetent mouse model to further identify immunosuppressive mechanisms and cell populations regulated by mCHMP2A activity. For this approach, the mCHMP2A gene was deleted using RNP-directed CRISPR-Cas9 gene editing in 4MOSC1 and 4MOSC2 HNSCC cell lines.[36] Three crRNA sequences were designed to target exon 1 of the mCHMP2A gene (online supplemental figure 1A). Transfection efficiency was greater than 90% in the 4MOSC1 and 4MOSC2 cell lines, as indicated by ATTO 550-labeled tracrRNA fluorescence (online supplemental figure 1B). Deletion of the mCHMP2A gene was confirmed with PCR and the lack of mCHMP2A protein expression was confirmed by immunoblot (online supplemental figure 1C). Clone B and C were further expanded and used for the rest of the experiment.

Loss of mCHMP2A in 4MOSC1 HNSCC increases sensitivity to mouse NK cell-mediated killing

To test murine NK cell antitumor activity against these cells, mouse NK cells were isolated from the C57Bl/6 (B6) mice and characterized by flow cytometry (online supplemental figure 2A). Isolated mouse NK cells were used in a standard cytotoxicity assay against 4MOSC1, 2WT and mCHMP2A KO tumor targets (figure 1A,B). Similar to previous studies using human NK cells against human tumor targets,[18] mouse NK cell-mediated killing activity against the mCHMP2A KO cells was notably increased for the 4MOSC1 mCHMP2A KO tumor target compared with the 4MOSC1 WT cells (figure 1A). In contrast, there was no difference in NK cell-mediated cytotoxicity between 4MOSC2 mCHMP2A KO and 4MOSC2 WT tumor cells (figure 1B).

4MOSC1 KO, but not 4MOSC2 KO, tumors spontaneously regress in vivo

To evaluate whether mCHMP2A KO increases tumor sensitivity to NK cells and other immune cells in vivo, we used a syngeneic mouse model. 4MOSC1 WT, 4MOSC1 mCHMP2A KO, 4MOSC2 WT, and 4MOSC2 mCHMP2A KO cells were implanted into the tongue of C57Bl/6 immunocompetent mice. Consistent with our data with mCHMP2A KO in vitro, mice bearing 4MOSC1 mCHMP2A KO cells showed spontaneous tumor regression in vivo. On day 16, mice injected with 4MOSC1 mCHMP2A KO tumor cells had an 85% smaller tumor volume on average than in mice injected with 4MOSC1 WT cells (figure 2A,C). However, 4MOSC2 mCHMP2A KO versus 4MOSC2 WT cells did not show any difference in tumor size in vivo (figure 2B). The average tumor volume for 4MOSC1 WT injected mice was 63.8 mm^3 while 4MOSC1 mCHMP2A KO injected mice had an average tumor volume of 9.49 mm^3 at the experimental endpoint (figure 2C). To validate that the mCHMP2A-mediated difference in tumor development is immune based, we challenged NOD.Cg-Prkdc^{scid}IL2rg^{tm1Wjl}/Sz (NSG) mice, which lack both the innate and adaptive lymphocytes, with
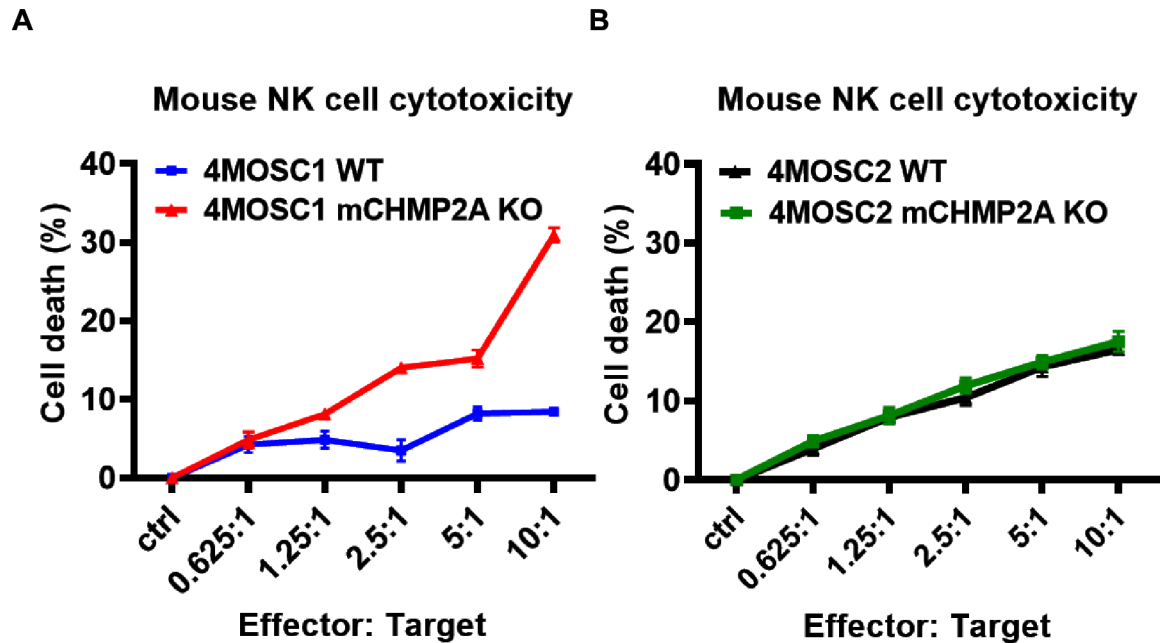
Figure 1 Deletion of mCHMP2A leads to increased NK cell cytotoxicity in vitro against 4MOSC1 cells, but not in 4MOSC2 tumor cells. (A) In vitro 4-hour cytotoxicity assay against 4MOSC1 WT and mCHMP2A KO cells. Mouse primary NK cells were used as effectors. Statistical analysis was performed by two-way ANOVA (10:1 p=0.0019; 5:1 p=0.0374; 2.5:1 p=0.0197 and 0.625:1 ns); and (B) cytotoxicity against 4MOSC2 WT and mCHMP2A KO cells. Statistical analysis was performed by two-way ANOVA (all E:T ratio ns). Data shown in (A, B), representative of n=2 independent experiments. ANOVA, analysis of variance; E:T, effector to target; KO, knock-out; NK, natural killer; WT, wild type.

4MOSC1 or 4MOSC2 WT compared with mCHMP2A KO tumors. Here, we observed no difference in the growth kinetics of WT versus KO tumors (figure 3A,B). This difference in tumor development between cells injected in C57Bl/6 versus NSG mice indicates there is increased immune-mediated rejection of the 4MOSC1 mCHMP2A KO compared with the WT cells. The mechanism for resistance in 4MOSC2 tumor has not been well established. However, our previous studies found 4MOSC2 tumors demonstrate elevated expressions of various chemokines (including CXCL1 and CXCL5) and growth factors such

as Granulocyte colony-stimulation factor (G-CSF) and Granulocyte-macrophage colony-stimulating factor (GM-CSF) in comparison to 4MOSC1 tumors.[36] This heightened expression potentially aids in the attraction and maintenance of MDSCs and inflammatory cells.[36 38]

Deletion of mCHMP2A leads to higher immune infiltration in 4MOSC1 tumors

On day 11 post-tumor injection, we isolated tumors and analyzed the infiltrating immune cell populations by immunofluorescence and flow cytometric analysis
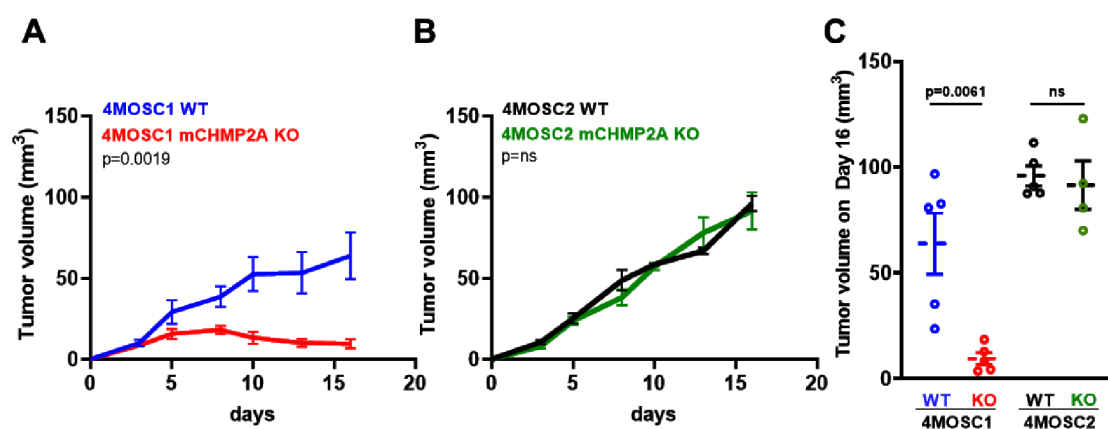

Figure 2 NK cell-mediated antitumor immunosurveillance is active in 4MOSC1 but not 4MOSC2 tumors. (A) C57BL/6 mice were implanted with 1×10^6 of 4MOSC 1 WT and 4MOSC 1 mCHMP2A KO cells into the tongue. Growth kinetic curves of 4MOSC1 tumor-bearing mice are shown as average tumor volumes (n=5 mice per group; two sited Student's t-test). (B) C57Bl/6 mice were implanted with 1×10^6 of 4MOSC2 WT and 4MOSC2 mCHMP2A KO cells into the tongue (n=5 mice per group, p=0.942). (C) Average tumor volumes on day 16 depicted (Individual dots represent volume of each tumor, n=5 mice per group). KO, knock-out; NK, natural killer; WT, wild type.
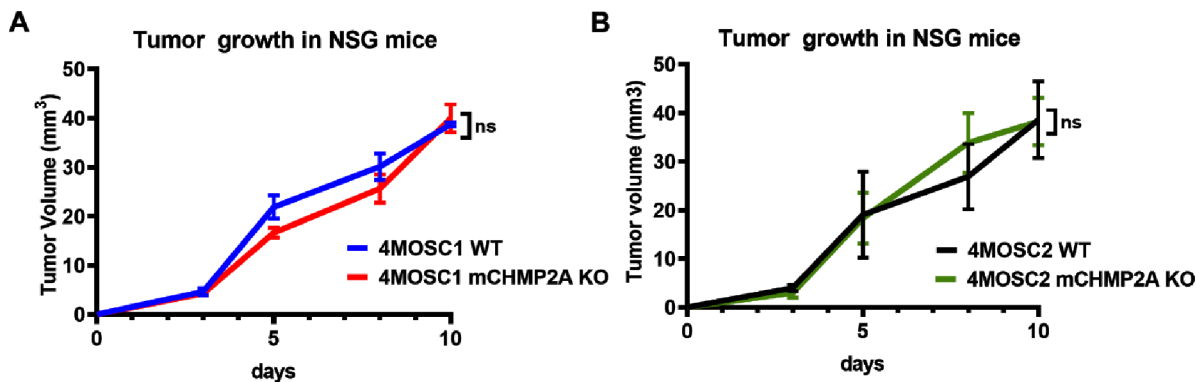
Figure 3 4MOSC1 and 4MOSC2 tumor growth in immunodeficient NSG mice. (A) NSG mice were implanted with 1×10^6 of 4MOSC 1 WT and 4MOSC 1 mCHMP2A KO cells into the tongue. Shown is the average volume of each tumor (n=5 mice per group; two-sided Student's t-test, p=0.868). (B) NSG mice were implanted with 1×10^6 of 4MOSC2 WT and 4MOSC2 mCHMP2A KO cells into the tongue. Shown is the average volume of each tumor (n=5 mice per group p=0.930). KO, knock-out; WT, wild type.

(online supplemental figure 2A,B). We found that the 4MOSC1 mCHMP2A KO tumors had significantly higher infiltration of NK, CD4+T, and CD8+T cells (figure 4). Specifically, 4MOSC1 mCHMP2A KO tumor tissue had 2.1-fold more CD4+ T cell (figure 4A) and 5.2-fold more CD8+ T cell (figure 4B) infiltration than what was seen in 4MOSC1 WT tumor tissue. Similarly, NK cells in 4MOSC1 mCHMP2A KO tumor tissue made up 1.45% of all cells while in WT tumors the average was 0.35%, nearly a fourfold difference (figure 4A). When combined with the tumor growth data, the higher infiltration of immune cells in 4MOSC1 mCHMP2A KO corresponded to a 4.6-fold smaller tumor volume than 4MOSC1 WT cells (figure 2A). The T cell and NK cell immune infiltration rate against tumor volume was plotted to analyze the correlation, resulting in a negative correlation between immune cell infiltration and tumor volume with an R^2 value of 0.9196 and 0.7298 for CD3+T cells and NK cells, respectively (online supplemental figure 3A,B). That is, increased infiltration of T cells and NK cells corresponds with smaller tumor volume. However, when comparing the immune infiltration in 4MOSC2 tumor tissue, no difference was observed between mCHMP2A KO and WT, consistent with there being no difference in tumor volume in 4MOSC2 mCHMP2A KO cells (figure 2B).

We also analyzed the infiltration of MDSC, characterized by CD11b+Ly6C- cells.[39] Here, we found that 4MOSC1 mCHMP2A KO tumors have less MDSC infiltration compared with 4MOSC1 WT tumors (figure 4D,H). Higher MDSC infiltration correlated with decreased T cell and NK cell infiltration and larger tumor volume in the 4MOSC1 mCHMP2A KO tumors. Plotting MDSC infiltration against tumor size resulted in a positive correlation with an R^2 value of 0.7846. (online supplemental figure 3C). Moreover, there is no significant change in MDSC infiltration of the 4MOSC2 mCHMP2A cells compared with 4MOSC2 WT cells (figure 4H). Again, these results with the 4MOSC2 tumors are consistent with our previous studies.

We further compared the infiltration of T cells and NK cells by immunofluorescence analysis. In parallel with the flow cytometric analysis, immunofluorescence staining demonstrates more abundant CD3+ and NK1.1+ cells, indicating higher infiltration of T cells and NK cells in 4MOSC1 mCHMP2A KO compared with 4MOSC1 WT (figure 5A–C). However, 4MOSC2 WT and mCHMP2A KO did not show a significant difference in either CD3+ and NK1.1+ cell infiltration (figure 5A–C). Notably, these studies demonstrate stronger fluorescence staining surrounding the outer side of the tumor in both 4MOSC2 WT and 4MOSC2 mCHMP2A KO tumors, indicating these tumors remain immunologically "cold" and less susceptible to immune cell infiltration, even with deletion of mCHMP2A. In contrast, mCHMP2A KO in 4MOSC1 tumors led to much more immune cell infiltration and tumor regression when compared with its WT counterpart.

Additional studies of cytokines and chemokines expressed by these WT and mCHMP2A KO tumors demonstrate that deletion of mCHMP2A in the 4MOSC1 tumors (mCHMP2A KO) leads to significantly higher levels of multiple cytokines and chemokines compared with the 4MOSC1 WT tumors (online supplemental figure 4A,B). Specifically, 4MOSC1 mCHMP2A KO tumor showed higher levels of proinflammatory cytokines/chemokines including CXCL10, CXCL12, IL2, and IL6, which may lead to attraction of immune cells and tumor regression in immune competent mice. While deletion of mCHMP2A in the 4MOSC2 tumors also led to slight increase in some cytokines and chemokines compared with the 4MOSC2 WT tumors, these changes were often not significant and more modest than the increase seen in the 4MOSC1 CHMP2A KO tumors (online supplemental figure 4A,B). Notably, consistent with previous results, 4MOSC2 tumors expressed higher levels of multiple chemokines (including CXCL1 and GM-CSF) compared with 4MOSC1 tumors.[36] This suggests that the regulation of the immune milieu is complicated by competing
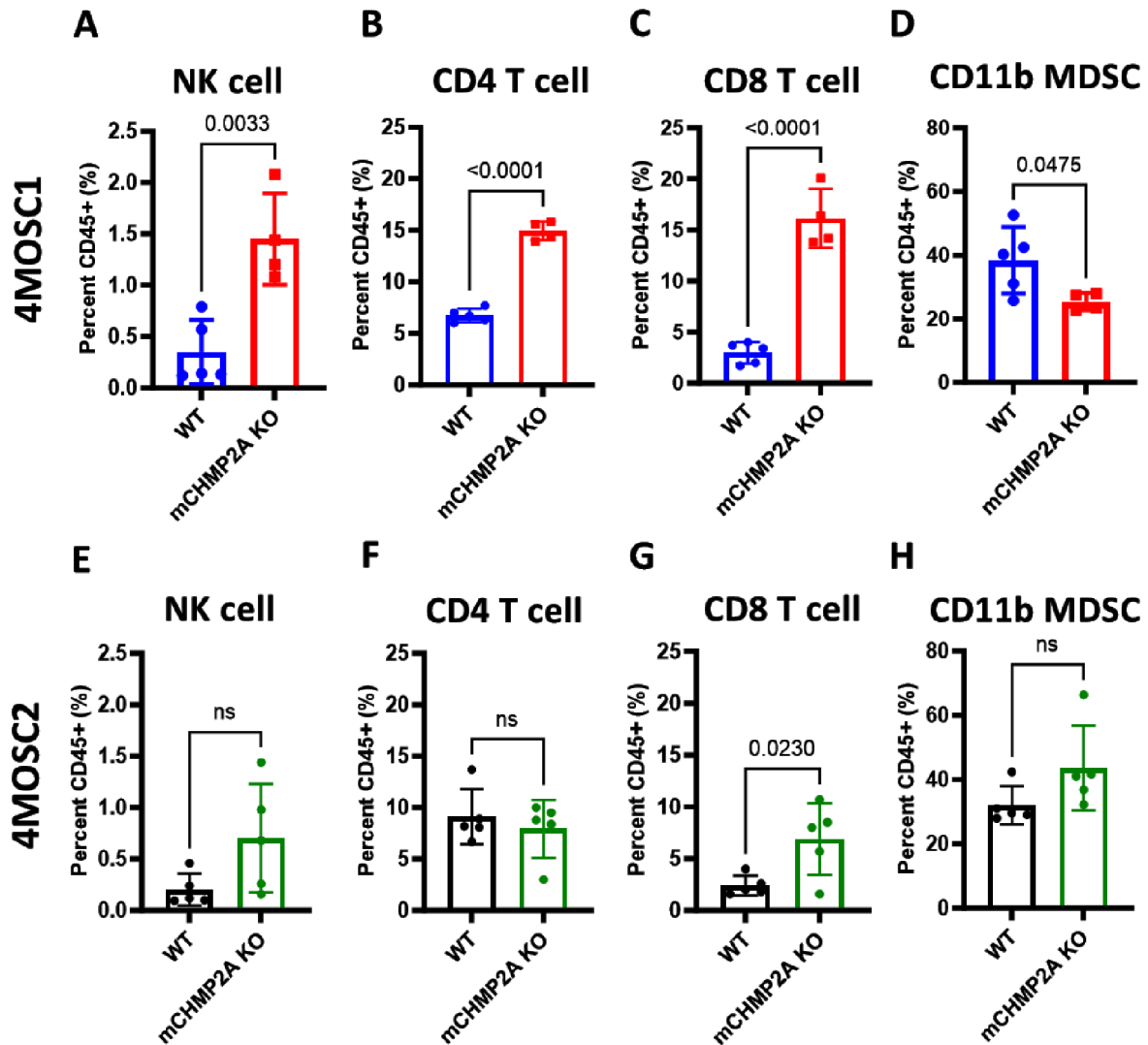
Figure 4 Infiltration of immune cells in 4MOSC tumor. C57BL/6 mice were implanted with 1×10⁶ of (A–D) 4MOSC1 (n=5 mice for WT n=4 mice for mCHMP2A KO, one mouse injected with mCHMP2A KO failed to show tumor engraftment). (E–H) 4MOSC2 WT or mCHMP2A KO cells into the tongue analyzed by flow cytometry of the tumors at day 11, showing the infiltration of (A, E) NK cells (B, F) CD4⁺ T cells (C, G) CD8⁺ T cells (D, H) CD11b⁺ MDSCs in tumors. KO, knock-out; MDSCs, myeloid-derived suppressor cells; NK, natural killer; WT, wild type.

immune regulatory factors, and further study is needed to determine the role of different chemokines to regulate immune response in HNSCC.

Depletion of immune cells diminishes antitumor activity against 4MOSC1 CHMP2A-KO tumors in vivo

To investigate the functional role of key immune effector cells in mediating the effect of mCHMP2A on the progression of 4MOSC1 tumors, we selectively depleted either CD8 T cells, CD4 T cells, and NK cells in vivo. As noted previously, untreated 4MOSC1 mCHMP2A KO tumor showed significantly smaller tumor volume compared with 4MOSC1 WT (figure 6A), 4MOSC1 KO treated with either anti-CD8 and anti-NK1.1 showed impaired anti-tumor activity (figure 6B,C). This shows that not only NK cells but also CD8⁺T cell activities mediate antitumor activity against the 4MOSC1 mCHMP2A KO tumor cells. However, when CD4⁺T cells were depleted, there was no

difference in tumor growth compared with untreated mCHMP2A KO (figure 6D), suggesting the effect of mCHMP2A activity such as cytokine and EV production[18] primarily inhibits cytotoxic lymphocytes. These results expand on the previous studies that demonstrate no reduction in growth of 4MOSC1 mCHMP2A KO tumors compared with WT tumors when injected into immuno-deficient NSG mice (figure 3).

EVs secreted by the 4MOSC cells express NKG2D ligands

Previous studies reported that EVs secreted by tumor cells express NKG2D ligands which binds to the activating receptor NKG2D on NK cells.[40] Accumulation of the EVs suppresses NK cell activity by binding to the NKG2D and TRAIL-R on NK cells causing fratricide or down modulating NKG2D.[40 41] Besides inhibiting NK cell activity, tumor-derived EVs suppress T cell activation and proliferation while stimulating apoptosis, and the
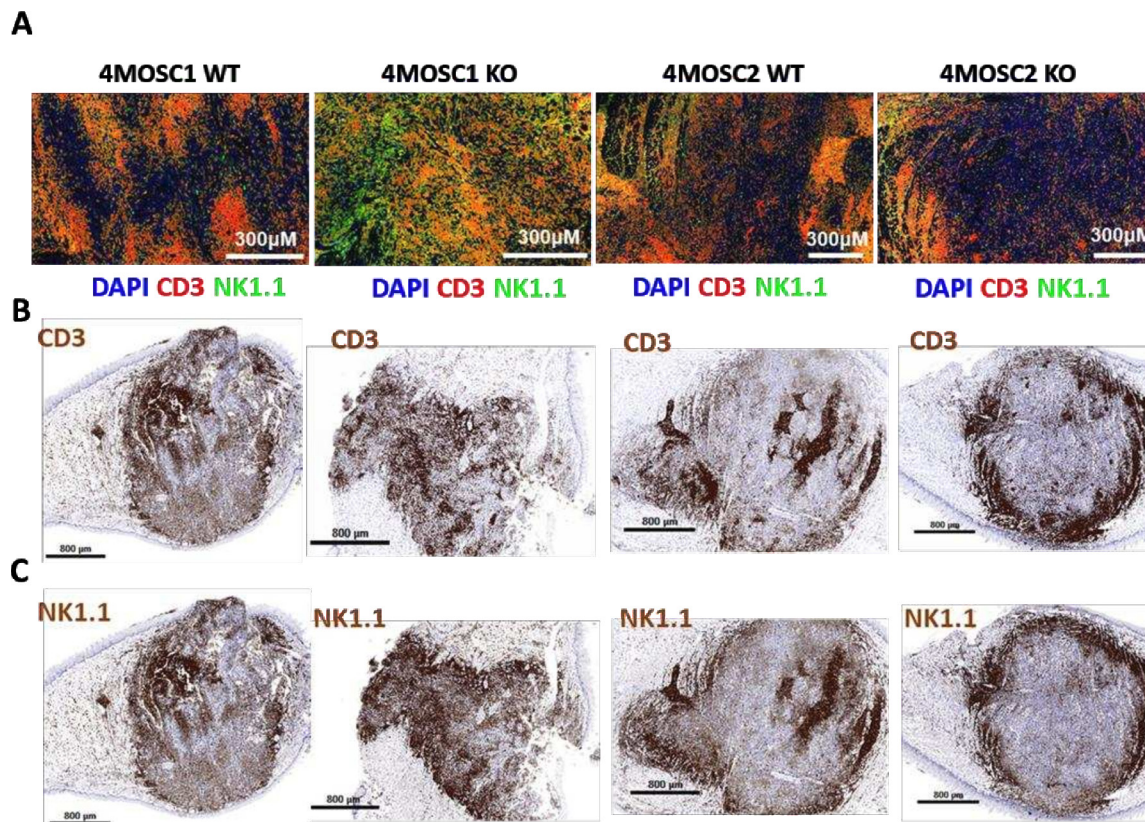
Figure 5 Difference in immune cell infiltration between 4MOSC WT and KO tumors. (A) Representative immunofluorescent staining of histological tissue sections from B6 mouse tongues with 4MOSC1 WT, 4MOSC1 KO, 4MOSC2 WT, and 4MOSC2 KO tumors on day 10 post injection. Images of stained tumors to show expression of CD3 (Red) NK1.1 (green) DAPI (blue). Immunostaining of CD3 and NK1.1 highlights an increase of CD45+CD3+ T cell and CD45+NK1.1+ NK cell recruitment in 4MOSC1 KO tumor compared with 4MOSC1 WT tumors. (B) Representative tumor tissue sections stained for CD3 by immunohistochemistry show increase in CD3+T cell infiltration in 4MOSC1 KO compared with 4MOSC1 WT but no significant difference in 4MOSC2 WT and 4MOSC2 KO tumors. (C) Immunohistochemistry staining for NK1.1 to show increase in NK cell infiltration in 4MOSC1 KO than in 4MOSC1 WT. No significant change in NK infiltration observed in 4MOSC2 WT and 4MOSC2 KO tumors. KO, knock-out; NK, natural killer; WT, wild type.

impact of tumor-derived EVs on T cells is influenced by the presence of FasL, TRAIL, membrane-bound TGFβ, CD73, or galectins on EVs.[42 43] To investigate the role of EVs on NK and T cells, we collected EVs from WT and 4MOSC mCHMP2A KO cells and analyzed expression of mouse NKG2D ligand mRae, mULBP, and mH60 by flow cytometry. EVs from both 4MOSC1 and 4MOSC2 WT and mCHMP2A KO tumors expressed mouse NKG2D ligands mRae, mULBP, and mH60 (figure 7A). Notably, there was no difference in the expression of the NK cell ligands between the WT and KO-tumor cells. This again demonstrates that 4MOSC cells secrete EVs with the ability to inhibit both NK cell and T cell-mediated cytotoxicity through the expression of NKG2D ligands and immunosuppressive molecules such as IL10 and TGF-β that have been demonstrated to be expressed in tumor EVs.[44] We have previously demonstrated that CHMP2A as part of the ESCRTIII regulates EV secretion and that KO of CHMP2A leads to production of fewer of these immune inhibitory EVs from human tumor cells.[18] However, there was no difference in the number and size of collected EVs between WT and mCHMP2A KO (online supplemental

figure 5A,B). This suggests that increase in antitumor activity in 4MOSC1 mCHMP2A KO cells is likely not due to decrease in the number of EVs but likely due to increased cytokine and chemokine expression. Other mechanisms such as impairment of perforin-mediated membrane holes may also play a role in increased killing of the 4MOSC1 mCHMP2A KO.[29]

DISCUSSION
Targeting solid tumors with cellular immunotherapies remains challenging.[45–47] One key contributing factor to tumor resistance is the inhibitory activity in the solid TME.[10 48–50] Our previous studies used a CRISPR/Cas9-mediated two-cell type screen to identify CHMP2A as a potent negative regulator of NK cell-mediated antitumor activity in both glioblastomas and HNSCC tumor cells.[18]

While these previous studies demonstrated the ability of CHMP2A deletion to increase NK cell-mediated antitumor activity in an NSG xenograft model, here we used a fully immune-competent mouse model to provide a more complete analysis of immune cell regulation by CHMP2A.
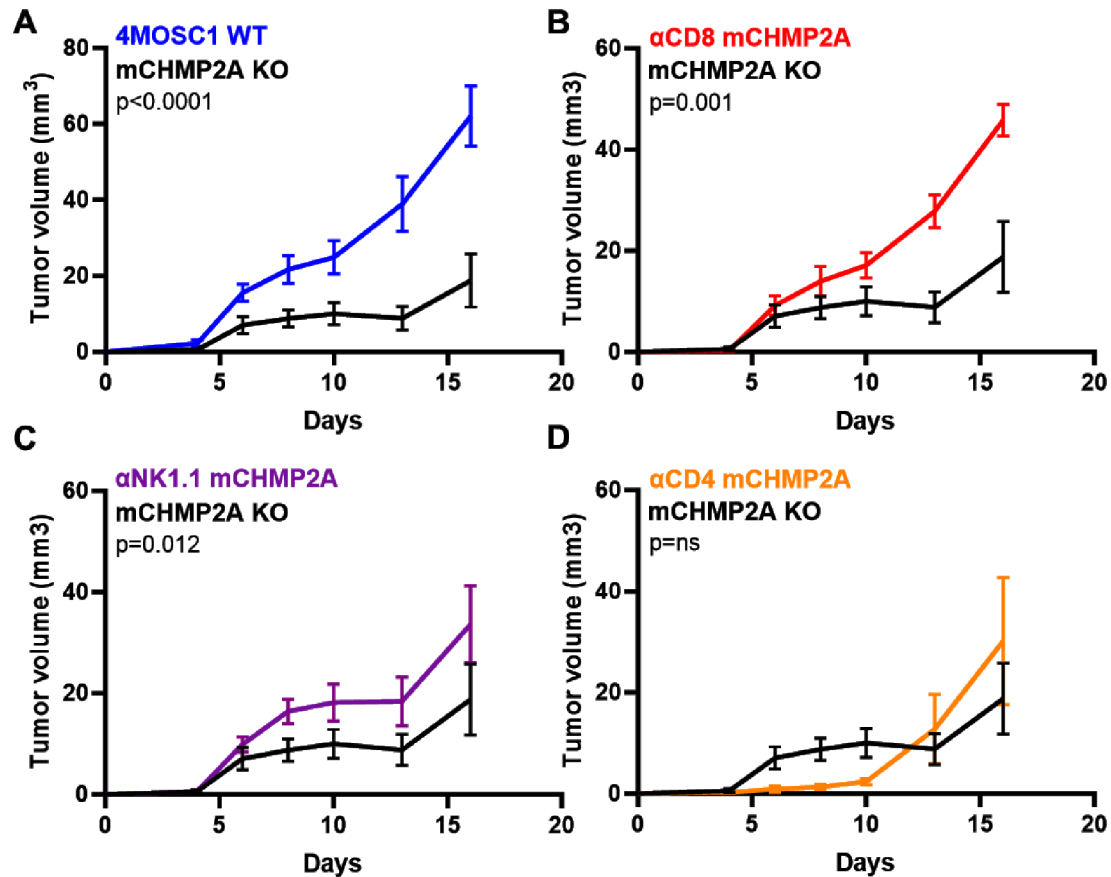
Figure 6 Depletion of immune cells reduces antitumor effect of mCHMP2A deletion on 4MOSC1 cells. (A) C57BL/6 mice were implanted with 1×10^6 of 4MOSC 1 mCHMP2A KO or 4MOSC1 WT cells into the tongue. Mice were treated with IP with 10 mg/kg of (B) anti-CD8 (C) anti-NK1.1 or (D) anti-CD4 (n = 7 per group). Individual growth curve of the 4MOSC1 mCHMP2A tumor-bearing mice are shown. KO, knock-out; NK, natural killer; WT, wild type.

Our data indicate that mCHMP2A deletion in mouse HNSCC tumors increases infiltration of not only NK cells but also $CD3^+$ T cells and NKT cells. Notably, we report a difference between 4MOSC1 and 4MOSC2 tumor cell lines. Although both lines were isolated from the same parental line, 4MOSC2 tumors exhibit a more aggressive phenotype, higher metastatic potential, and greater resistance to anti-CTLA-4 and anti-PD-1 therapy compared with the 4MOSC1 tumors.[36–38] Notably, the 4MOSC2 tumors demonstrate increased MDSC infiltration, a process that is not different when comparing 4MOSC2 CHMP2A KO versus WT cells (figure 5). Chemokine and cytokine analysis of these tumors demonstrated that the 4MOSC1 mCHMP2A KO tumors exhibited elevated levels of proinflammatory cytokines (eg, CXCL10 and CXCL12) compared with the 4MOSC1 WT tumors, likely resulting in increased immune infiltration (online supplemental figure 4, figure 4A–C and figure 5). This T cell and NK cell infiltration can mediate the antitumor immune response against the 4MOSC1 mCHMP2A KO tumors and lack of tumor progression in the immune competent mice (figure 2B). These results are also consistent with our findings that depletion of either NK cells or CD8+cells leads to increased tumor growth of the 4MOSC1 mCHMP2A KO tumors in the immune competent mice

(figure 6). Notably, the 4MOSC2 mCHMP2A KO tumors do not have the same significant increase in proinflammatory cytokines and chemokines compared with the 4MSOC2-WT tumors (online supplemental figure 4). This corresponds to the lack of increased T cell and NK cell infiltration in these tumors (figure 4F,G) and lack of tumor regression of the 4MOSC2 mCHMP2A KO tumors in the immune competent mice. Additional studies testing these mCHMP2A KO and WT tumors in immunodeficient NSG mice further demonstrate that mCHMP2A mediates immune resistance, as there is no difference in tumor growth in the immunodeficient mice (figure 3). Importantly, the deletion of mCHMP2A in 4MOSC1 cells led to intense immune infiltrates, whereas the 4MOSC2 mCHMP2A KO tumors remained immunologically cold without an increase in infiltrating immune cells (figures 4 and 5).

CHMP2A is part of the ESCRT-III complex that regulates membrane remodeling including extracellular vesicle (EV) biogenesis, multivesicular formation, and membrane repair.[21 29] There are several mechanisms by which CHMP2A loss may lead to more immune infiltration of tumors. Deletion of CHMP2A in tumor cells activates the NF-κB pathway, increasing the release of chemokines including CXCL10 and CXCL12, which stimulate the
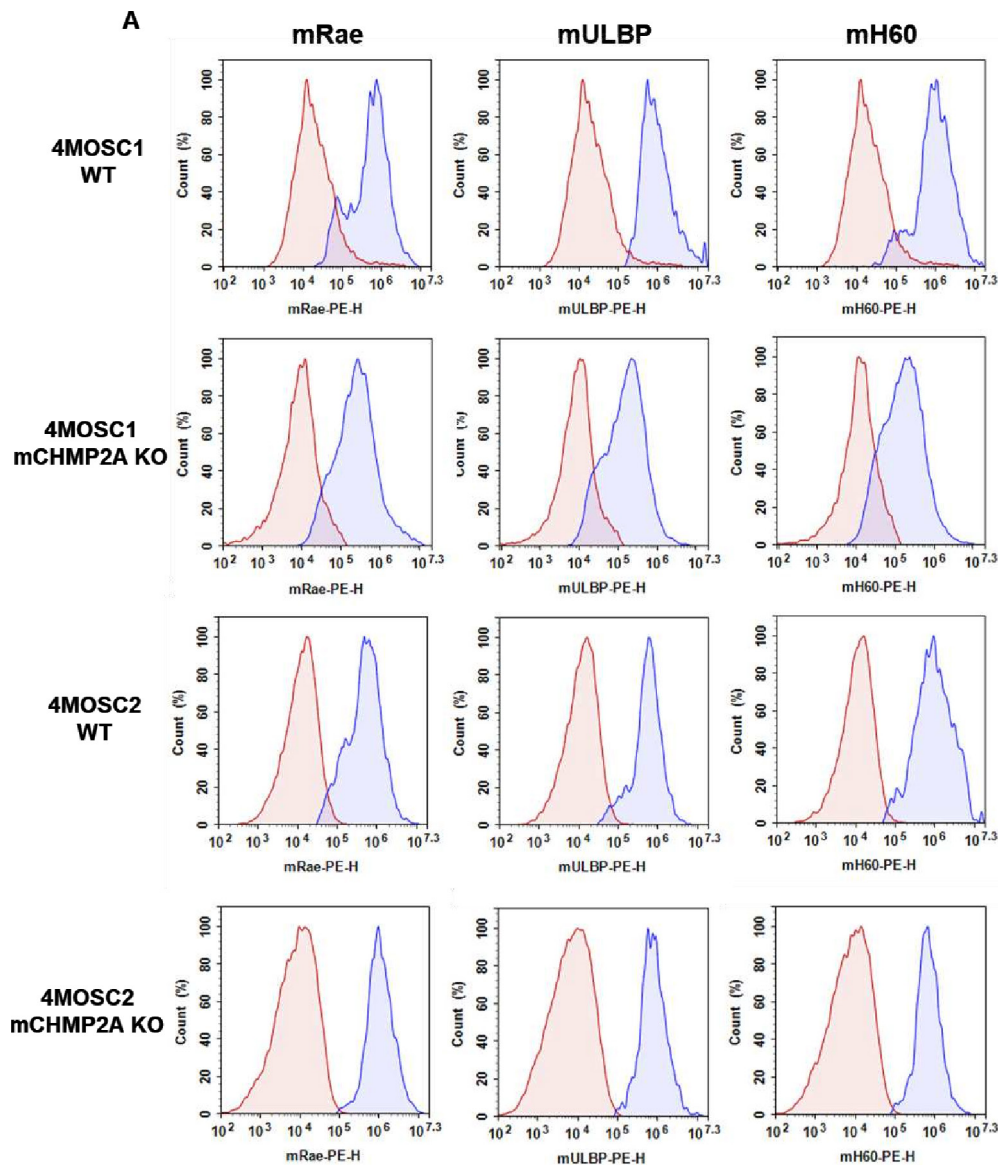
Figure 7 EVs secreted by 4MOSC cell lines express mouse NKG2D ligands. (A) 4MOSC1 and 4MOSC2 WT and mCHMP2A KO derived EVs were collected and analyzed by flow cytometry for mouse NKG2D ligands mRae, mULBP, mH60 (blue histogram). Red histogram represents isotype. EVs, extracellular vehicles; KO, knock-out.

migration of NK cells and T cells to tumor cells.[18 51 52] Additionally, EV secretion is regulated by the ESCRT-III complex and loss of CHMP2A leads to fewer immune inhibitory EVs secreted from tumor cells.[18] Another possible mechanism is via the protection of tumor cells from perforin released by cytotoxic T cells and NK cells. Both cytotoxic T cells and NK cells release perforin to open a pore in target cells which allows the entrance of granzymes, resulting in apoptosis of the target cell.[21 29 53] Once the cell membrane lesion is created by perforin, ESCRT proteins gather to facilitate repair, thus allowing target cells to escape from T cell and NK cell-mediated cytotoxicity.[29] Supporting this idea, recent studies demonstrate that inhibition of the ESCRT pathway increased sensitivity to T cell-mediated and NK cell-mediated cytotoxicity.[18 29] Notably, CHMP2A KO in the 4MOSC1 and 4MOSC2 cells did not lead to quantitative changes in EV production as

was seen in the human tumors.[18] These results indicate that main mechanism of increased immune sensitivity of the 4MOSC1-KO cells is more likely due to the increased production of the proinflammatory cytokines that lead to recruitment of the NK cells and CD8+T cells. Again, impaired repair of perforin-mediated membrane holes may also play a role in increased killing of the 4MOSC1 mCHMP2A KO.[29]

Together, these studies demonstrate the development of a drug or a small molecule to target CHMP2A or other ESCRT proteins can likely improve the efficacy of checkpoint inhibitors and prevent resistance against T cell and NK cell-mediated immunotherapies.

ORCID iDs
Jiyoung Yun http://orcid.org/0009-0004-4513-0201
Robert Saddawi-Konefka http://orcid.org/0000-0002-9936-1695
Dan Kaufman http://orcid.org/0000-0002-2003-2494

REFERENCES

1. Abel AM, Yang C, Thakar MS, *et al*. Natural killer cells: development, maturation, and clinical utilization. *Front Immunol* 2018;9:1869.
2. Vivier E, Tomasello E, Baratin M, *et al*. Functions of natural killer cells. *Nat Immunol* 2008;9:503–10.
3. Goh W, Huntington ND. Regulation of murine natural killer cell development. *Front Immunol* 2017;8:130.
4. Wagner AK, Alici E, Lowdell MW. Characterization of human natural killer cells for therapeutic use. *Cytotherapy* 2019;21:315–26.
5. Shah K, Al-Haidari A, Sun J, *et al*. T cell receptor (TCR) signaling in health and disease. *Signal Transduct Target Ther* 2021;6:412.
6. Gascoigne NRJ, Rybakin V, Acuto O, *et al*. TCR signal strength and T cell development. *Annu Rev Cell Dev Biol* 2016;32:327–48.
7. He Q, Jiang X, Zhou X, *et al*. Targeting cancers through TCR-peptide/MHC interactions. *J Hematol Oncol* 2019;12.
8. Zhong S, Malecek K, Johnson LA, *et al*. T-cell receptor affinity and avidity defines antitumor response and Autoimmunity in T-cell Immunotherapy. *Proc Natl Acad Sci USA* 2013;110:6973–8.
9. Paul S, Lal G. The molecular mechanism of natural killer cells function and its importance in cancer Immunotherapy. *Front Immunol* 2017;8:1124.
10. Giraldo NA, Sanchez-Salas R, Peske JD, *et al*. The clinical role of the TME in solid cancer. *Br J Cancer* 2019;120:45–53.
11. Raulet DH, Guerra N. Oncogenic stress sensed by the immune system: role of natural killer cell receptors. *Nat Rev Immunol* 2009;9:568–80.
12. Pende D, Falco M, Vitale M, *et al*. Killer IG-like receptors (Kirs): their role in NK cell modulation and developments leading to their clinical exploitation. *Front Immunol* 2019;10:1179.
13. Ruggeri L, Capanni M, Casucci M, *et al*. Role of natural killer cell Alloreactivity in HLA-Mismatched hematopoietic stem cell transplantation. *Blood* 1999;94:333–9.
14. Kärre K. Natural killer cell recognition of missing self. *Nat Immunol* 2008;9:477–80.
15. Luo XR. Missing self triggers NK cell-mediated chronic vascular rejection of solid organ transplants. *Transplantation* 2020;104:448–9.
16. Nayyar G, Chu Y, Cairo MS. Overcoming resistance to natural killer cell based Immunotherapies for solid tumors. *Front Oncol* 2019;9:51.
17. Sordo-Bahamonde C, Vitale M, Lorenzo-Herrero S, *et al*. Mechanisms of resistance to NK cell Immunotherapy. *Cancers (Basel)* 2020;12:893.
18. Bernareggi D, Xie Q, Prager BC, *et al*. Chmp2A regulates tumor sensitivity to natural killer cell-mediated cytotoxicity. *Nat Commun* 2022;13:1899.
19. Teis D, Saksena S, Emr SD. Ordered assembly of the ESCRT-III complex on endosomes is required to sequester cargo during MVB formation. *Dev Cell* 2008;15:578–89.
20. Alqabandi M, de Franceschi N, Maity S, *et al*. The ESCRT-III Isoforms Chmp2A and Chmp2B display different effects on membranes upon polymerization. *BMC Biol* 2021;19:66.
21. Hattori T, Takahashi Y, Chen L, *et al*. Targeting the ESCRT-III component Chmp2A for Noncanonical Caspase-8 activation on Autophagosomal membranes. *Cell Death Differ* 2021;28:657–70.
22. Kalluri R, LeBleu VS. The biology, function, and BIOMEDICAL applications of Exosomes. *Science* 2020;367.
23. Stoten CL, Carlton JG. ESCRT-dependent control of membrane remodelling during cell division. *Semin Cell Dev Biol* 2018;74:50–65.
24. Ferrari de Andrade L, Kumar S, Luoma AM, *et al*. Inhibition of MICA and MICB shedding elicits NK-cell-mediated immunity against tumors resistant to cytotoxic T cells. *Cancer Immunol Res* 2020;8:769–80.
25. Singh S, Banerjee S. Downregulation of HLA-ABC expression through promoter Hypermethylation and Downmodulation of MIC-A/B surface expression in Lmp2A-positive epithelial carcinoma cell lines. *Sci Rep* 2020;10.
26. Raulet DH, Gasser S, Gowen BG, *et al*. Regulation of ligands for the Nkg2D activating receptor. *Annu Rev Immunol* 2013;31:413–41.
27. Hedlund M, Nagaeva O, Kargl D, *et al*. Thermal- and oxidative stress causes enhanced release of Nkg2D ligand-bearing immunosuppressive Exosomes in leukemia/lymphoma T and B cells. *PLoS One* 2011;6:e16899.
28. Xing S, Ferrari de Andrade L. "Nkg2D and MICA/B shedding: a 'tag game' between NK cells and malignant cells". *Clin Transl Immunology* 2020;9:e1230.
29. Ritter AT, Shtengel G, Xu CS, *et al*. ESCRT-mediated membrane repair protects tumor-derived cells against T cell attack. *Science* 2022;376:377–82.
30. Charap AJ, Enokida T, Brody R, *et al*. Landscape of natural killer cell activity in head and neck squamous cell carcinoma. *J Immunother Cancer* 2020;8:e001523.
31. Sun XZ, Zhang LJ, Liu SJ. The immune infiltration in HNSCC and its clinical value: A comprehensive study based on the TCGA and GEO databases. *Comput Math Methods Med* 2021;2021:1163250.
32. Weil S, Memmer S, Lechner A, *et al*. Natural killer group 2d ligand depletion Reconstitutes natural killer cell Immunosurveillance of head and neck squamous cell carcinoma. *Front Immunol* 2017;8:387.
33. Chen Y, Li Z-Y, Zhou G-Q, *et al*. An immune-related gene Prognostic index for head and neck squamous cell carcinoma. *Clin Cancer Res* 2021;27:330–41.
34. Baysal H, De Pauw I, Zaryouh H, *et al*. Cetuximab-induced natural killer cell cytotoxicity in head and neck squamous cell carcinoma cell lines: investigation of the role of Cetuximab sensitivity and HPV status. *Br J Cancer* 2020;123:752–61.
35. Mandal R, Şenbabaoğlu Y, Desrichard A, *et al*. The head and neck cancer immune landscape and its Immunotherapeutic implications. *JCI Insight* 2016;1:e89829.
36. Wang Z, Wu VH, Allevato MM, *et al*. Syngeneic animal models of tobacco-associated oral cancer reveal the activity of in situ anti-CTLA-4. *Nat Commun* 2019;10:5546.

37 Saddawi-Konefka R, O'Farrell A, Faraji F, *et al*. Lymphatic-preserving treatment sequencing with immune Checkpoint inhibition Unleashes Cdc1-dependent antitumor immunity in HNSCC. *Nat Commun* 2022;13:4298.

38 Wang Z, Goto Y, Allevato MM, *et al*. Disruption of the Her3-Pi3K-mTOR Oncogenic signaling axis and PD-1 blockade as a Multimodal precision Immunotherapy in head and neck cancer. *Nat Commun* 2021;12:2383.

39 Lv M, Wang K, Huang XJ. Myeloid-derived suppressor cells in hematological malignancies: friends or foes. *J Hematol Oncol* 2019;12:105.

40 Vulpis E, Loconte L, Peri A, *et al*. Impact on NK cell functions of acute versus chronic exposure to extracellular vesicle-associated MICA: dual role in cancer Immunosurveillance. *J Extracell Vesicles* 2022;11:e12176.

41 Vulpis E, Loconte L, Cassone C, *et al*. Cross-dressing of multiple myeloma cells mediated by extracellular vesicles conveying MIC and ULBP ligands promotes NK cell killing. *Int J Mol Sci* 2023;24:9467.

42 Ma F, Vayalil J, Lee G, *et al*. Emerging role of tumor-derived extracellular vesicles in T cell suppression and dysfunction in the tumor microenvironment. *J Immunother Cancer* 2021;9:e003217.

43 Gutiérrez-Vázquez C, Villarroya-Beltri C, Mittelbrunn M, *et al*. Transfer of extracellular vesicles during immune cell-cell interactions. *Immunol Rev* 2013;251:125–42.

44 Reale A, Khong T, Spencer A. Extracellular vesicles and their roles in the tumor immune microenvironment. *J Clin Med* 2022;11:6892.

45 Hou AJ, Chen LC, Chen YY. Navigating CAR-T cells through the solid-tumour microenvironment. *Nat Rev Drug Discov* 2021;20:531–50.

46 Lamb MG, Rangarajan HG, Tullius BP, *et al*. Natural killer cell therapy for hematologic malignancies: successes, challenges, and the future. *Stem Cell Res Ther* 2021;12:211.

47 Marofi F, Al-Awad AS, Sulaiman Rahman H, *et al*. CAR-NK cell: a new paradigm in tumor Immunotherapy. *Front Oncol* 2021;11:673276.

48 Erin N, Grahovac J, Brozovic A, *et al*. Tumor Microenvironment and epithelial Mesenchymal transition as targets to overcome tumor multidrug resistance. *Drug Resist Updat* 2020;53:100715.

49 Khalaf K, Hana D, Chou JT-T, *et al*. Aspects of the tumor Microenvironment involved in immune resistance and drug resistance. *Front Immunol* 2021;12:656364.

50 Deepak KGK, Vempati R, Nagaraju GP, *et al*. Tumor Microenvironment: challenges and opportunities in targeting metastasis of triple negative breast cancer. *Pharmacol Res* 2020;153:104683.

51 Kurowarabe K, Endo M, Kobayashi D, *et al*. Cxcl12-stimulated lymphocytes produce secondary stimulants that affect the surrounding cell Chemotaxis. *Biochem Biophys Rep* 2021;28:101128.

52 Jin J, Zhao Q. Emerging role of mTOR in tumor immune Contexture: impact on Chemokine-related immune cells migration. *Theranostics* 2020;10:6231–44.

53 Rubin TS, Zhang K, Gifford C, *et al*. Perforin and Cd107A testing is superior to NK cell function testing for screening patients for genetic HLH. *Blood* 2017;129:2993–9.